Georgopoulou *et al.*
Functional Composite Materials (2022) 3:9
https://doi.org/10.1186/s42252-022-00037-5

Functional Composite Materials

RESEARCH

Open Access

Thermoplastic elastomer composite strips with damage detection capabilities for self-healing elastomers

Antonia Georgopoulou[1,2*], Henry Korhonen[1], Anton W. Bosman[3] and Frank Clemens[1*]

Abstract

Self-healing materials can increase the lifetime of products and improve their sustainability. However, the detection of damage in an early stage is essential to avoid damage progression and ensure a successful self-healing process. In this study, self-healing sensor composite strips were developed with the embedding of a thermoplastic styrene-based copolymer (TPS) sensor in a self-healing matrix. Piezoresistive TPS sensor fibers composites (SFCs) and 3D printed sensor element composites (SECs) were fabricated and embedded in a self-healing matrix by lamination process to detect damage. In both cases, the value of the initial resistance was used to detect the presence of damage and monitor the efficiency of healing. A higher elongation at fracture could be achieved with the extruded sensor fibers. However, for the composite strips the SECs could achieve a higher elongation at fracture. Mechano-electrical analysis revealed that the strips maintained a monotonic, reproducible response after the healing of the matrix. The SFCs had significantly lower drift of the sensor signal during cyclic mechanical analysis. Nevertheless, on a tendon-based soft robotic actuator, the SECs obtained a drift below 1%. This was explained by the lower deformation (e.g.) strain in comparison to the tensile test experiments.

Introduction

Self-healing polymers can heal repeatedly when damage occurs and therefore, they increase the lifetime of future polymeric products and decrease the number of waste products [1]. Nowadays, the development of self-healing materials is crucial for reaching sustainability goals and reducing the carbon dioxide footprint of our modern societies [2]. In order to ensure that the self-healing is successful, detecting the damage early is essential. Nociception is a function of the natural organisms to receive the stimulus of pain triggered by different factors like damage and inflammation [3]. Nociception is an important element of the adaptation and evolution of life, as it can protect organisms from dangerous conditions that could harm them [4, 5]. Additionally, the process of nociception can trigger a series of events for natural organisms, associated with the defensive and healing process [6, 7]. In self-healing polymer structures, like artificial soft robotic systems, the function of nociception can be mimicked by piezoresistive sensors. Piezoresistive sensors can be used to detect damage and monitor when the healing process has been successfully achieved [8–10]. Moreover, the integration of a piezoresistive sensor allows to determine the actual position of the robot limbs [10, 11] and closed-loop control of robotic movements [12, 13].

In order to avoid stiffening the soft robot structure, a composite approach can be used for developing composite strips [14–16]. These composite structures are developed with the integration of the functional element, in the form of a single thread, in a soft elastomeric matrix material [12, 17]. The resulting composite strip is

*Correspondence: antonia.georgopoulou@empa.ch; frank.clemens@empa.ch

[1] Department of Functional Materials, Empa – Swiss Federal Laboratories for Materials Science and Technology, Überlandstrasse 129, 8600 Dübendorf, Switzerland
Full list of author information is available at the end of the article

functional and can maintain the softness of the matrix material. For self-healing materials, similar concept can be used to combine self-healing properties with the functionality derived from the sensor thread [18, 19].

Piezoresistive elastomer-based sensors with self-healing properties have been recently developed. However, there are some limitations for composite elastomers with self-healing capability. Georgopoulou et al. used self-healing piezoresistive sensors for developing composite strips, detect the damage and monitor the motion of a robotic actuator [10]. However, the sensitivity and drift of the sensor were inferior to the properties reported for piezoresistive soft composites without self-healing properties and further investigation is needed to be able to use self-healing sensors for motion monitoring applications. In addition, in the same study, a filler of 30 wt.% resulted in a significantly diminished elongation at the point of fracture for the self-healing elastomer UPy1 (e.g. from 1200 to 70%) [10]. Similar results have been reported by others [20–23]. Khimi et al. reported a lower self-healing efficiency of at least one third, by adding of carbon black filler [24]. Unfortunately, after self-healing the elongation at the point of fracture for the UPy1 dropped further down, below 30% [10]. Han et al. observed that after each self-healing cycle, the elongation at break decreased for their carbon nanotube—latex based self-healing sensor material [25]. Similar results were reported by Liu et al. and Dai et al. for their carbon nanotubes based self-healing conductive elastomers after a few cycles of damage and healing [26, 27].

Thus, we propose there is still potential for using non self-healing sensors to monitor self-healing soft material structures. The self-healing process is activated by heat and therefore, non self-healing sensors with high melting point above 160 °C are able to withstand the accelerated healing process by thermal treatment. In this study, we demonstrate how self-healing composite strips can be made by combining a self-healing matrix with sensors, like fibers or 3D printed sensor elements based on styrene-based tri-block copolymer (TPS). Commercial 3D printers with screw extruder printing heads have been successfully used for the fabrication of piezoresistive sensors with low drift and good sensitivity [28, 29]. In order to integrate the sensing elements in the self-healing matrix, casting methods [30–32] or lamination [12, 33] have been reported in literature. The goal is to see if the sensors can detect the presence of damage in the self-healing matrix of the composite strip and compare the sensor response between fibers and 3D printed elements. Two different piezoresistive sensor composites and matrix materials will be used. The mechano-electrical analysis was evaluated before and after the thermal treatment required for the healing of the elastomer matrix. The mechanical and electrical behavior of sensor fibers, 3D printed elements and composite strips are evaluated and compared for their piezoresistive behavior after being embedded in the self-healing matrix materials. Finally, detecting damage and self-healing of the matrix material will be performed during tensile testing and for composite strips attached to a tendon-based soft robotic actuator.

Material and methods

Preparation of piezoresistive sensors based on thermoplastic elastomer composite

A styrene-based tri-block co-polymer (TPS) was obtained by Kraiburg TPE (Waldkraiburg, Germany) in Shore hardness 40A and 50A. The two types of TPS will be called TPS 40A and TPS 50A in this study. Carbon black Ensaco 250 was obtained from Imerys (Paris, France). As described in details elsewhere, both TPS thermoplastic elastomers were mixed in a 1:1 weight ratio with the carbon black filler, using a torque rheometer from Thermofisher (Polylab, Karlsruhe, Germany) and extruded into filament by capillary rheometer from Netzsch (RHSelb, Germany) [34, 35].

Preparation of the composite piezoresistive sensor fibers

To evaluate the piezoresistive properties of the two TPS composites, composite sensor fibers were extruded using a Voladora Nx + (International Technology 3D Printers S.L., Valencia, Spain) pellet printer. The nozzle used for the extrusion had a 0.8 mm diameter. Further details have been reported elsewhere [29, 36].

Preparation of the piezoresistive composite sensor elements

For the self-healing element composite strips, composite sensor elements with dimensions of $130 \times 1.2 \times 0.4$ mm were printed with the Voladora Nx + FDM pellet printer, as described previously [28]. The temperature used for heating zone 1 and heating zone 2 was 220 °C and 250 °C, respectively. A printing speed of 15 mm/s and a temperature of 45 °C for the printing bed were used. The extrusion multiplier was set to 45 and 40 for the piezoresistive composites based on TPS 50A and 40A, respectively. A thin polytetrafluoroethylene (PTFE) foil (Polyfluor, Breda, Netherlands) was placed on the printing bed to ensure the good adhesion of the piezoresistive-sensing elements (Fig. 1).

Preparation of the sensorized self-healing composite strips

As shown in Fig. 2, the printed piezoresistive sensing elements were laminated between two self-healing polymer films. The films were made of UPy1 and UPy2 from

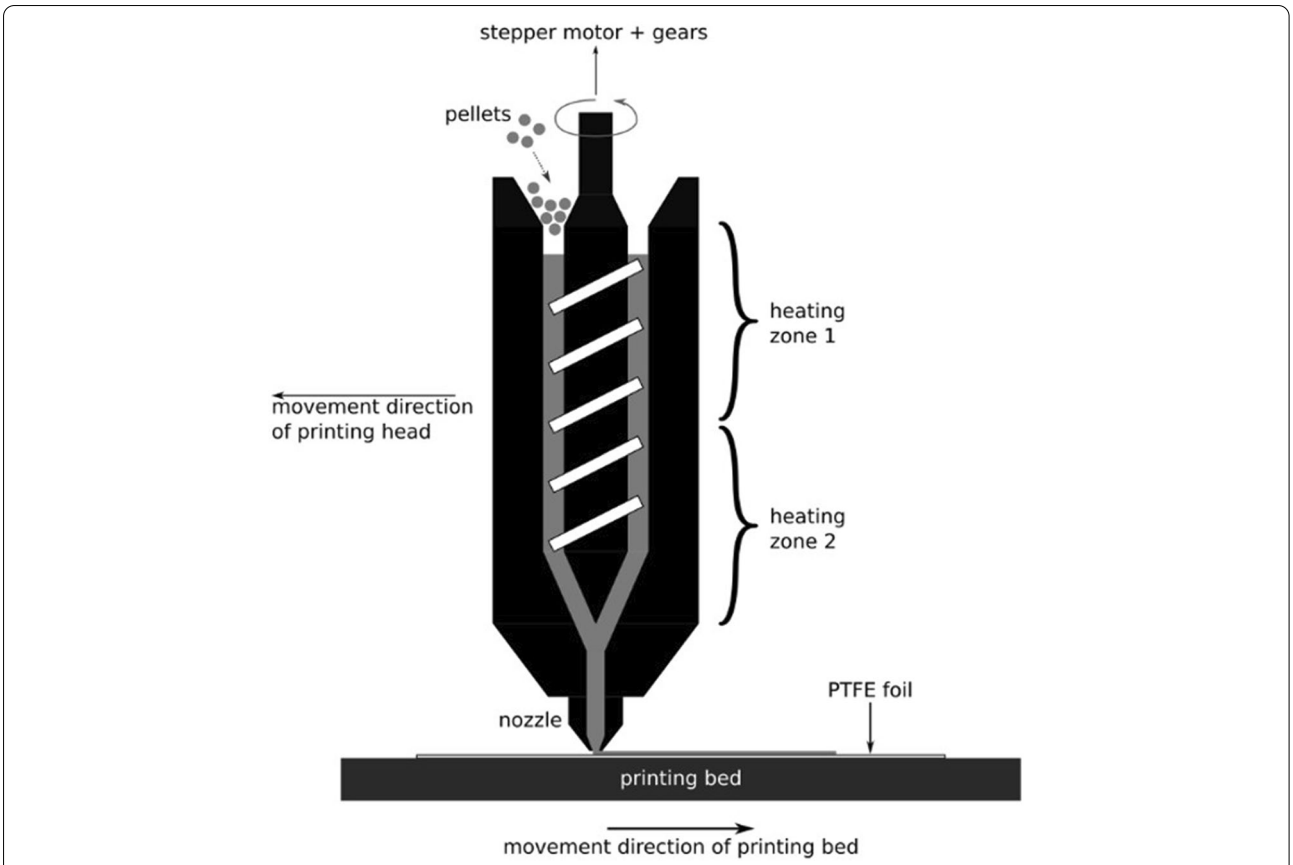

Fig. 1 The fabrication of the composite piezoresistive sensor elements with pellet-based FDM

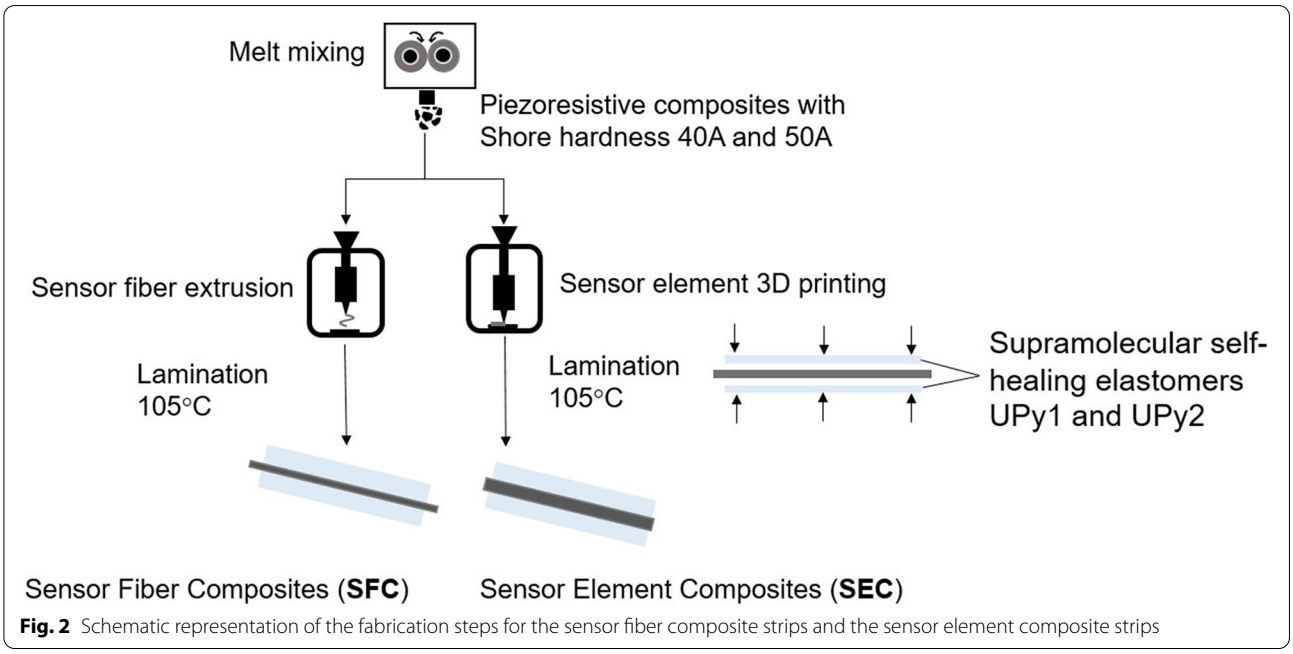

Fig. 2 Schematic representation of the fabrication steps for the sensor fiber composite strips and the sensor element composite strips

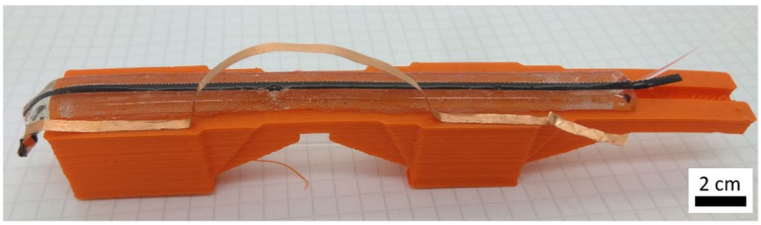

Fig. 3 Soft robotic actuator with attached sensorized self-healing composite strips. Cooper tape was used to connect the end of the piezoresistive elements with electrical cables

SupraPolix BV (Eindhoven, The Netherlands). These self-healing elastomers comprise ureido-pyrimidinone (UPy) units as reversible hydrogen bonded cross-links and for UPy1 comprise additionally a hydrogenated polybutadiene polyol backbone, and for UPy2 a poly(tetramethylene oxide) backbone [10]. The self-healing behavior of both elastomers was based on the UPy quadruple hydrogen bonds [37].

The self-healing elastomers were hot pressed (Fontijne Press, Delft, The Netherlands) into a 0.7 mm thick film at 120 °C and 150 N. For the preparation of sensorized self-healing composite strips, films of the UPy1 and UPy2 elastomers were cut into pieces with a length of 100 mm and a width of 7 mm. 3D printed piezoresistive sensing elements were placed in between two elastomer films. To fuse the two films, the composite strips had to be placed in a furnace (Memmert, Schwabach, Germany). At 105 °C for 10 min. To verify the fusing process composite strips were investigated under the optical microscope using the microscope Discovery from Carl Zeiss AG (Jenna, Germany).

The resulting composite strips will be called sensor fiber composite strips (SFC) and sensor element composite strips (SEC) for the fiber and printed element integration, respectively.

Evaluation of self-healing composite strips for soft robotic actuator modules

Self-healing sensitized soft actuator modules in robotics are of high interest nowadays [38, 39]. However, raw material and synthesis of self-healing elastomers is still a cost and time related issue. Therefore, due to the limited amount of self-healing elastomer films, the sensor and self-healing behavior of the composite strips were investigated on TPU based soft robotic actuator modules. The tendon-based soft robotic actuator modules were 3D printed using a thermoplastic polyurethane (TPU) filament with Shore hardness 90A from Spectrum Group (Pecice, Poland) and a filament-based FDM 3D printer Voladora Nx + (International Technology 3D Printers S.L., Valencia, Spain). The actuators were equipped with a stainless steel tendon wire of 0.5 mm diameter. For the actuation of the tendon-based soft robotic module, a Dynamixel AX-12A servomotor from Robotis (Lake Forest, Illinois, USA) and an Arduino microcontroller were used. The self-healing sensorized composite strips were attached to the surface of the soft robotic actuators using Sil-Poxy silicone glue from Smooth-ON.

(Macungie, Pennsylvania, USA). To contact the end of the piezoresistive sensing elements with electrical cables a commercial copper tape (3 M, Maplewood, USA), as shown in Fig. 3.

Characterization of the Mechano-Electrical Behavior with tensile testing

Tensile testing of the extruded piezoresistive fiber sensors was carried out on a Zwick & Roell Z005 tensile testing machine (Zwick & Roell GmbH & Co., Ulm, Germany). The electrical signal was recorded with a Keithley 2450 multimeter (Keithley Instruments, Solon, OH, USA). Dynamic properties were investigated by cyclic tensile testing, using 10 cycles between 0 and 50% strain and a strain rate of 200 mm/s. During the cycling test, the electric resistance was recorded with a sampling rate of 10 Hz. Data were presented as mean values ± standard deviation with sample size ($n = 3$). In order to investigate the damage detection capabilities of the piezoresistive sensing element inside the self-healing matrix, cuts of 0.3 mm were performed in the middle of the strips on both sides. The dynamic analysis was performed on pristine composite strips (before the damage), after damage and after healing the matrix material. The healing was performed at 105 °C for 10 min, and an interval of 48 h was always chosen between the heat-activated healing process and the mechano-electrical testing.

The relative resistance (R_{rel}) was calculated using the following formula:

$$R_{rel} = \frac{R - Ro}{Ro} \tag{1}$$

And the Gauge Factor (GF) was calculated with the following formula:

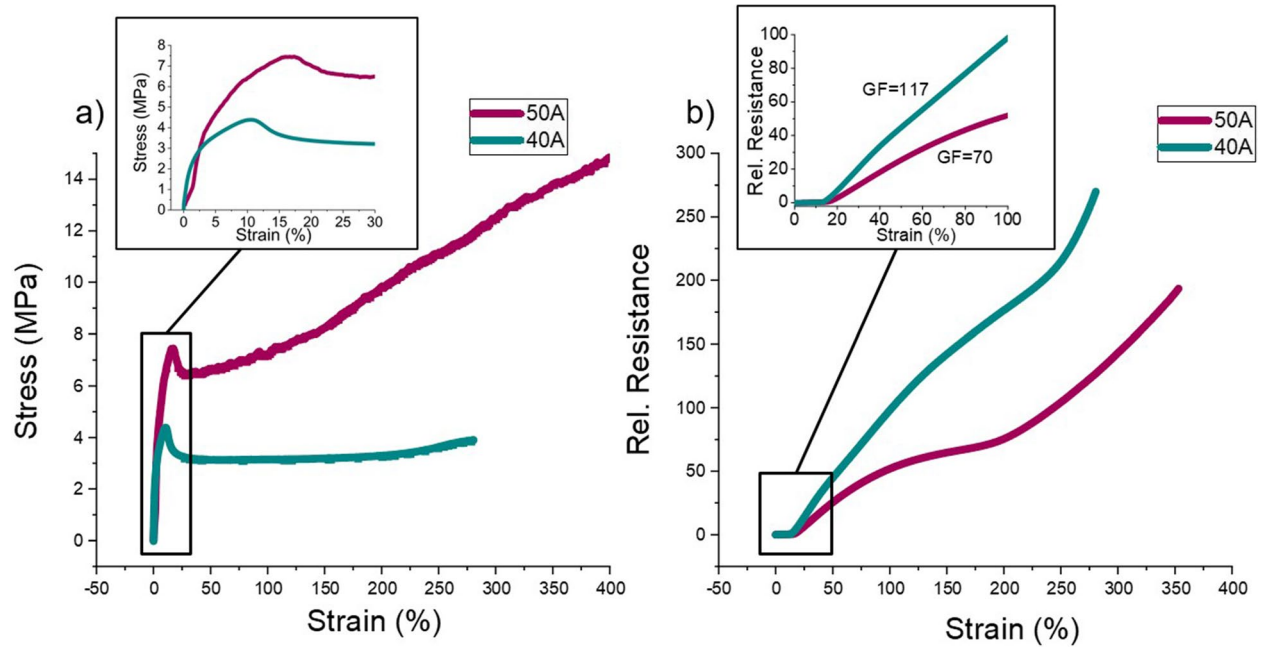

Fig. 4 **a** Stress–strain curve and **b** relative resistance curve during the tensile test up to the point fracture for the two composite sensor fibers based on TPS matrix 40A and 50A

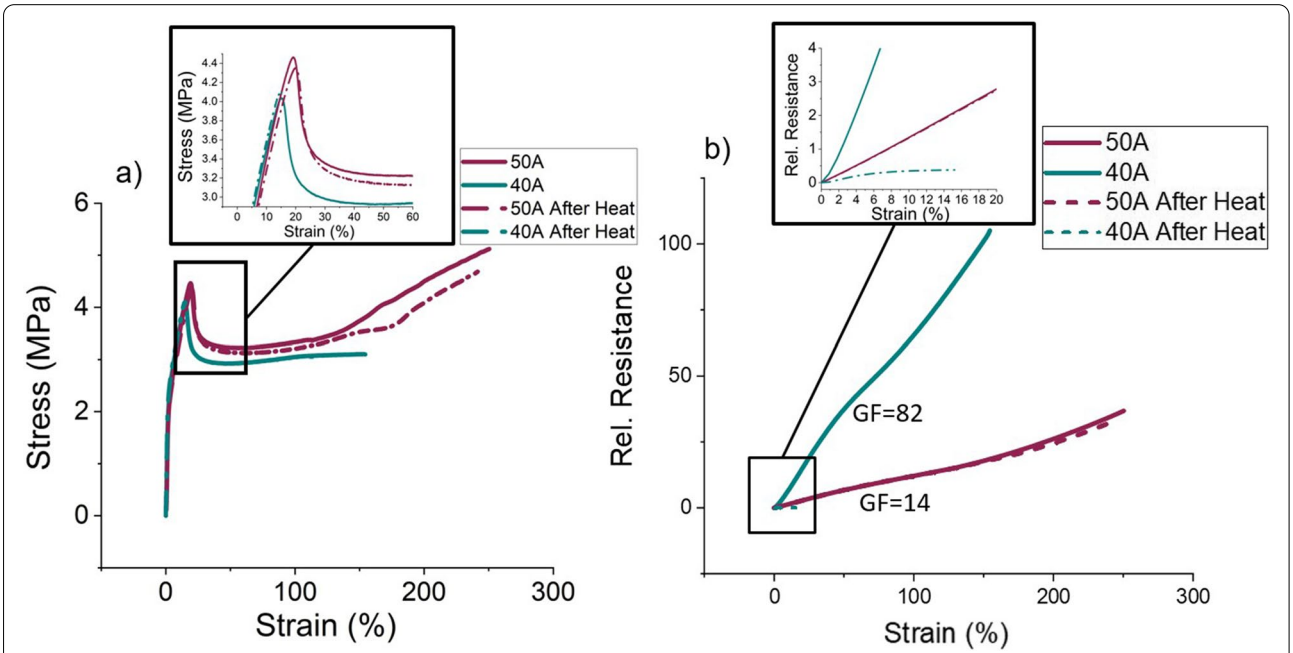

Fig. 5 **a** Stress–strain curve and **b** relative resistance curve during the tensile test up to the point fracture for the printed composite sensor elements based on the two TPS matrix materials with a Shore hardness 40A and 50A, before and after the thermal treatment at 105 °C for 30 min

$$GF = \frac{\Delta R_{rel}}{\Delta \varepsilon} \quad (2)$$

Results and discussion

Mechano-electrical behavior of piezoresistive fibers and 3D printed elements

The two different TPS composite sensor fibers were characterized with tensile testing up to the point of fracture. From the response of the stress (Fig. 4a), it was seen that both fibers showed the characteristic necking that has been already reported for styrene-based tri-block co-polymer (TPS) composites with higher filler content [34, 36, 40].

As for the yield point, it appeared at strain 10.3% for the fiber based on TPS 40A and 17.3% for the sensor fiber based on TPS 50A. Both fibers exhibited a strain hardening effect that was more prominent for the sensor fiber based on 50A. It had both a higher elongation at the point of fracture (400%) and larger ultimate strength (14.8 MPa). In comparison, the sensor fiber based on TPS 40A only reached an elongation of 270% (point of fracture) and 3.9 MPa (ultimate strength). These findings are in agreement with the results of a previous study that showed that decreasing the Shore hardness, below 50A, leads to a decrease in the point of fracture for TPS/CB sensor fibers [28].

Up to 20% strain, the electrical response is similar for both sensor fibers (Fig. 4b). For both fibers, the sensitivity increased significantly for strains above the yield point. A gauge factor (GF) of 117 and 70 was calculated between 20–100% strain for the sensor fibers based on TPS 40A and 50A, respectively. Similar behavior has been reported earlier for styrene-based tri-block co-polymer (TPS) carbon black composites with higher filler content [28].

Similar tensile tests were performed for the printed sensor elements. Because of the later lamination process at 105 °C, the elements were tested before and after heating at 105 °C. Comparing the elements based on TPS 40A and 50A, it can be seen that the sensor element based on TPS 50A could endure larger elongations (up to 250%) and had a higher ultimate strength of 5.12 MPa (Fig. 5a). The Young's modulus was calculated 1.58 MPa and 1.06 MPa for the 40A and 50A element respectfully. In an older study, it was reported that the Young's Modulus was 0.6 MPa for the elastomer UPy1 and 3.3 MPa for the elastomer UPy2. The sensor element based on TPS 40A could endure elongations of up to 151% and the tensile strength was 3.1 MPa. Comparing the sensor elements with the sensor fibers, it can be seen that the ultimate strength was lower for the sensor elements. The elongation at the point of fracture also decreased for the sensor elements but the strain hardening effect is also present for the sensing element based on TPS 50A.

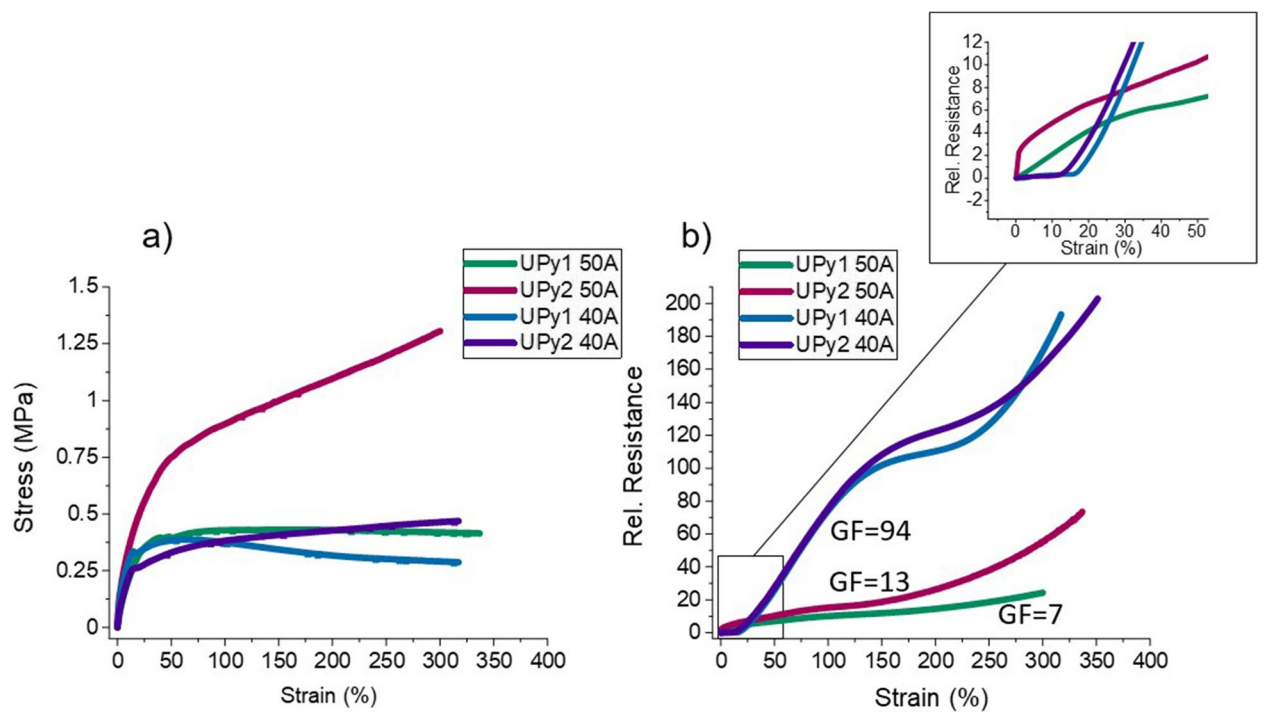

Fig. 6 **a** Stress–strain curve and **b** relative resistance curve for the self-healing sensor fiber composites (SFCs) with the supramolecular elastomers UPy1 and UPy2 for the TPS sensor fibers with Shore hardness 40A and 50A during the tensile test up to the point fracture

After the thermal treatment, the mechanical properties of the sensor element based on TPS 50A did not change significantly. The elongation at the point of fracture was 238% and the ultimate strength was 4.63 MPa. This was not the case for the sensor element based on TPS 40A. The elements broke at 14% strain, after the thermal treatment. Thus, the sensor composite based on TPS 40A is incompatible with self-healing matrix materials that require thermal treatment for healing.

For the relative resistance response, both sensor elements showed a positive piezoresistive response (Fig. 5b). It can be observed that lower Shore hardness resulted in a higher sensitivity (GF = 82), which is in good agreement with Fig. 4b. The GF is lower for the sensor elements, compared to the sensor fibers. The response of the sensor signal (relative resistance) of the sensing element based on TPS 50A looks almost identical before and after heating.

Mechano-electrical behavior of the fiber composite strips (SFCs)

After the analysis of the sensor fibers, the two fibers were embedded into two different self-healing supramolecular elastomers (UPy1 and UPy2). The mechanical and electrical characterization was repeated for the self-healing sensor fiber composite strips (SFC). From the response to the stress (Fig. 6a), it was seen that the SFC UPy2 50A had a higher ultimate strength (1.1 MPa) than the other SFCs (ca 0.3 MPa). The elongation at the point of fracture was similar for all the SFCs (ca 300%). The two SFCs, with the UPy1 matrix, exhibited a negative slope for strains higher than 50%. The strain hardening behavior that was seen in Fig. 4a does not appear for all the SFCs. A local decrease in the cross section was observed for the SFC UPy1 SFCs. Generally, elastomers have a viscoelastic behavior and the negative slope and decrease in cross-section are good indications that at higher strains,

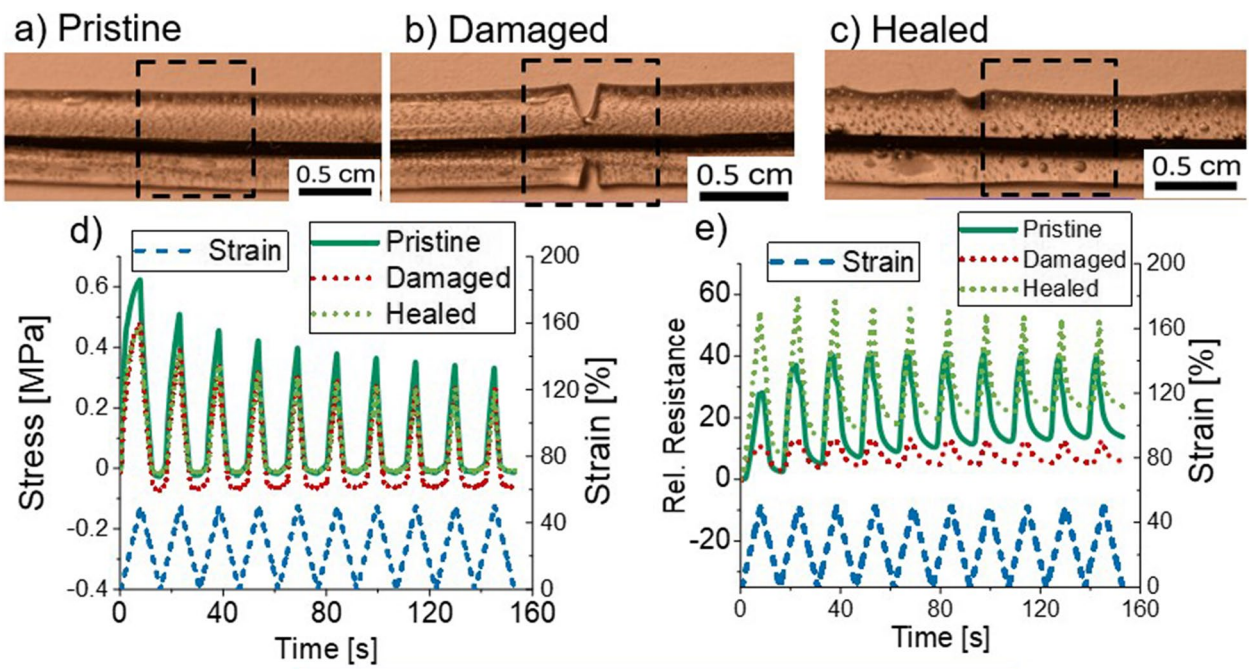

f)

	Pristine	Damaged	Healed
R_0 (kΩ)	6.7 ± 0.1	15.6 ± 0.6	18.2
ΔR_{rel}	28.5 ± 2.2	8.7 ± 0.4	27
Drift R_{rel} 5-10 cycle (%)	14.8 ± 0.8	13.2 ± 0.8	24.1

Fig. 7 Optical microscopy analysis of the SFC based on the supramolecular matrix UPy1 and the sensor fiber based on TPS 40A **a**) Pristine **b**) Damaged and **c**) Healed. Plots for the response of the **d**) Stress and **e**) Relative resistance **f**) Summary of the values for the R_0, ΔR_{rel} and the drift of the sensor signal between the 5th and 10th for the samples: pristine, damaged and healed. Because many samples broke after healing, it was not possible to obtain a representative standard deviation

the viscous behavior dominates the mechanical behavior of both SFCs with UPy1 matrix. Additionally, the elongation at the point of fracture increased slightly (20%) for both the SFCs 40A compared to the strain sensor fiber based on TPS 40A. The opposite trend was observed for the fiber based on TPS 50A, as both the SFCs 50A had an elongation at a break 100% smaller than the fiber based on TPS 50A.

For the relative resistance (Fig. 6b), in this case, the SFCs with the fiber based on TPS 40A, showed significantly higher sensitivity. This observation correlated with the analysis for the extruded sensor fibers shown in Fig. 4. The response was only linear for strains 20–140% and for strains above 250%. Looking at low strains, it can be seen that the SFCs with the fiber based on TPS 40A showed a plateau (no change in the slope) of the curve. This was not the case for the fiber based on TPS 50A which showed a positive slope at low strains. Comparing the GF in the range 0–100%, it can be seen that the value is identical (94) for the two 40A SFCs and 7 and 13 for the SFCs UPy1 50A and UPy2 50A, respectively. From these values, it is not evident if the matrix materials affect the electrical response, but it seems that in contrast to the response of the stress, for the electrical properties the sensor fiber plays the dominant role. The value is smaller than the GF of the sensor fibers, before the integration in the self-healing matrix. Looking at low strains (below 20%), it was not possible to calculate the GF, because the SFCs didn't exhibit a linear response, but it is evident that the SFCs 50A responded with higher sensitivity (ΔRrel), compared to the SFCs 40A with both self-healing matrix materials. The SFCs 40A shows a sensitive response for strains above 20%.

In order to investigate the reproducibility of the sensor response, dynamic cyclic tensile tests between 0–50% strains were performed for the four different SFCs. The dynamic cycling tests were repeated after the introduction of manual cuts from both edges (e.g. damage stage)

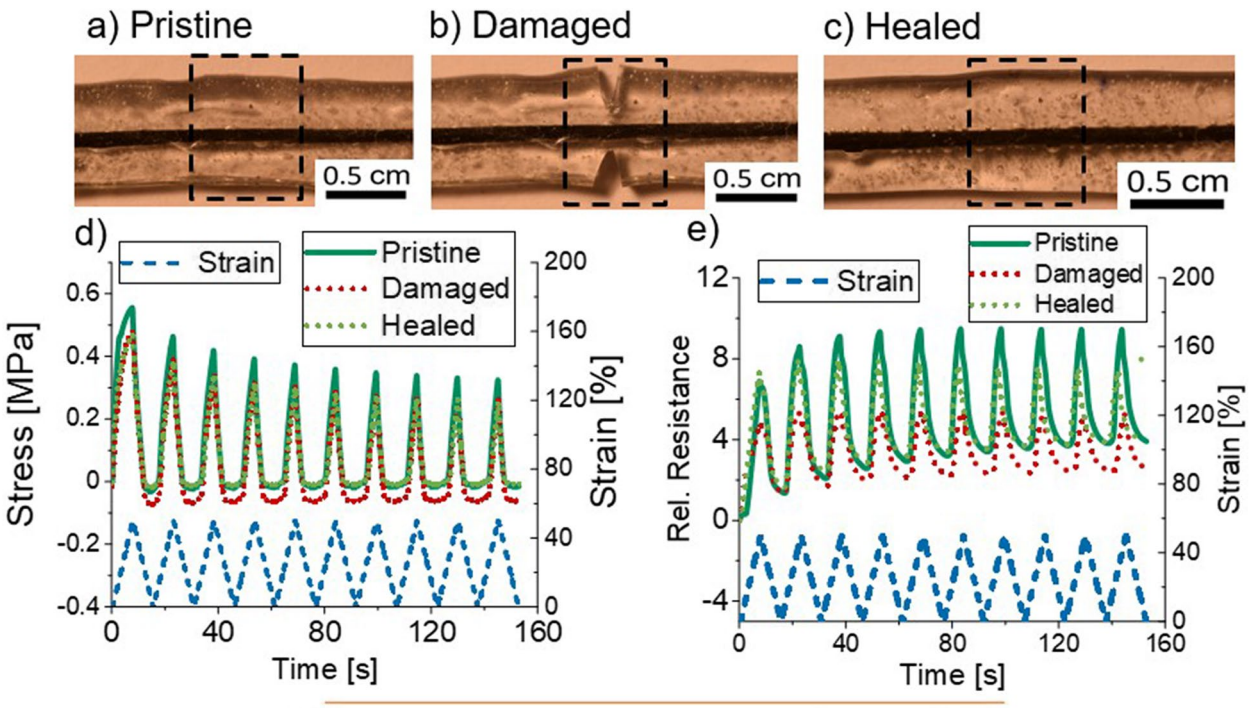

f)

	Pristine	Damaged	Healed
R_0 (kΩ)	4.4 ± 0.4	5.6 ± 0.1	4.3 ± 0.1
ΔR_{rel}	5.2 ± 0.4	3.1 ± 0.3	6 ± 0.7
Drift R_{rel} 5-10 cycle (%)	8.4 ± 1.8	7.7 ± 0.5	18 ± 1

Fig. 8 Optical microscopy analysis of the SFC based on the supramolecular matrix UPy1 and the sensor fiber based on TPS 50A **a**) Pristine **b**) Damaged and **c**) Healed. Plots for the response of the **d**) Stress and **e**) Relative resistance **f**) Summary of the values for the R_0, ΔR_{rel} and the drift of the sensor signal between the 5th and 10th for the samples: pristine, damaged and healed

and after healing. Figure 6 shows the results of the dynamic cycling tests. The optical microscope analyses for each stage (pristine, damaged, healed) are presented in (Fig. 7a, b, c).

For the stress curve in the damage stage (Fig. 7d), negative stress values can be observed after unloading (e.g. 0% strain), especially after the damage occurred. However, after healing, the values resembled the stress curve of the pristine one. The electrical response of the sensor signal was reproducible between the 2nd and 10th cycle for all three cases (Fig. 7e). The initial resistance (R_0) increased significantly when the damage occurred by manual cutting (Fig. 7f). After healing a similar sensitivity (ΔR_{rel}) can be observed however, the sensor signal was shifted to higher values due to the higher initial resistance and a re-calibration is needed. It is worthwhile to mention that the drift of the sensor signal increased significantly after self-healing process.

In Fig. 8a-f, the results of the SFC based on UPy1 and the sensor fiber based on TPS 50A are summarized. The mechanical behavior of this composite is similar to the one before (Fig. 8d). It can be concluded that the different Shore hardness of the two sensor fibers does not significantly affect the stiffness of the composite strips and the mechanical behavior (recovery of stress after the healing) is dominated by the self-healing UPy1 matrix material. As expected by the previous results, the sensitivity (ΔR) decreased with the higher Shore hardness value of the sensor fiber matrix. Unlike the SFC UPy1 40A, the SFC UPy1 50A doesn't need a recalibration after self-healing. Similar to the previous UPy1 matrix composite the relative resistance and the sensitivity decrease with the damage. After self-healing, the sensor revealed the same electrical signal behavior as the pristine one. However, the drift significantly increased after the heating and this is a disadvantage for this SFC (Fig. 8e and f).

For both SFCs based on UPy1 matrix, a change in electric signal behavior was observed. However, without additional AI (artificial intelligence) methods to cope

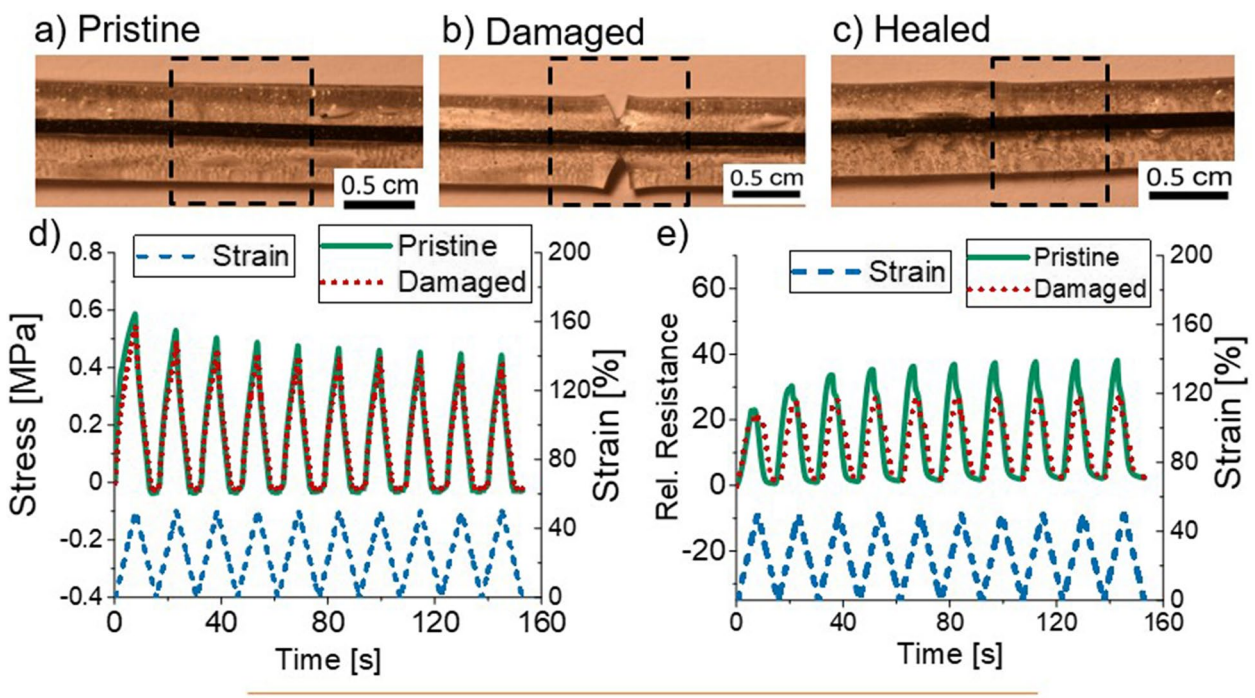

f)

	Pristine	Damaged	Healed
R_0 (kΩ)	1.8 ± 0.1	3.1 ± 0.3	(Samples Broke)
ΔR_{rel}	33.3 ± 2.1	6.4 ± 0.3	-
Drift R_{rel} 5-10 cycle (%)	2.5 ± 1.5	2.3 ± 1.6	-

Fig. 9 Optical microscopy analysis of the SFC based on the supramolecular matrix UPy2 and the sensor fiber based on TPS 40A **a**) Pristine **b**) Damaged and **c**) Healed. Plots for the response of the **d**) Stress and **e**) Relative resistance **f**) Summary of the values for the R_0, ΔR_{rel} and the drift of the sensor signal between the 5th and 10th for the samples: pristine, damaged and healed

with the drift behavior, it will be not possible to detect the damage and self-healing of the composite strip easily.

The dynamic tensile testing results for the UPy2 matrix composites with the two different sensor fibers are presented in Figs. 9a-f and 10a-f. Unfortunately, the SFCs with the TPS sensor fiber based on Shore hardness 40A were too brittle after the self-healing step to obtain any data from the dynamic testing (Fig. 9). The R_0 increased significantly but sensitivity (ΔR_{rel}) did not show a significant change after damage, which is in good agreement with previous results of the UPy1 SFCs. It is worthwhile to mention that the mechanical behavior of pristine and damaged samples are very similar. However, it can be concluded that the combination of UPy2 matrix and sensor fiber based on TPS 40A did not result in a composite material with intrigued damage detection.

From the response of the mechanical stress (Fig. 9d), it was seen that the profile of the stress was the same before and after the damage occurred. This is different from what was observed for the fiber SFCs with the UPy1 matrix, confirming again that the profile of the stress is dominated by the type of matrix material. As for the electrical response (Fig. 9e), the same response for the R_0 and ΔR_{rel} was seen, as for the other SFCs. The R_0 increased and ΔR_{rel} decreased after the damage occurred. No significant difference in the drift was observed after the healing.

Only the stress–strain behavior changed after damage and self-healing (Fig. 10). The negative stress in the pristine samples can be explained by the viscoelastic behavior of the UPy2, already reported in previous studies [12, 17]. The sensor signal did not show significant changes between pristine, damaged and healed stages (Fig. 10e). Therefore, only the value of the R_0 can be used for detecting the presence of damage. Similar to the SFC UPy1 50A, a re-calibration is not necessary after the healing.

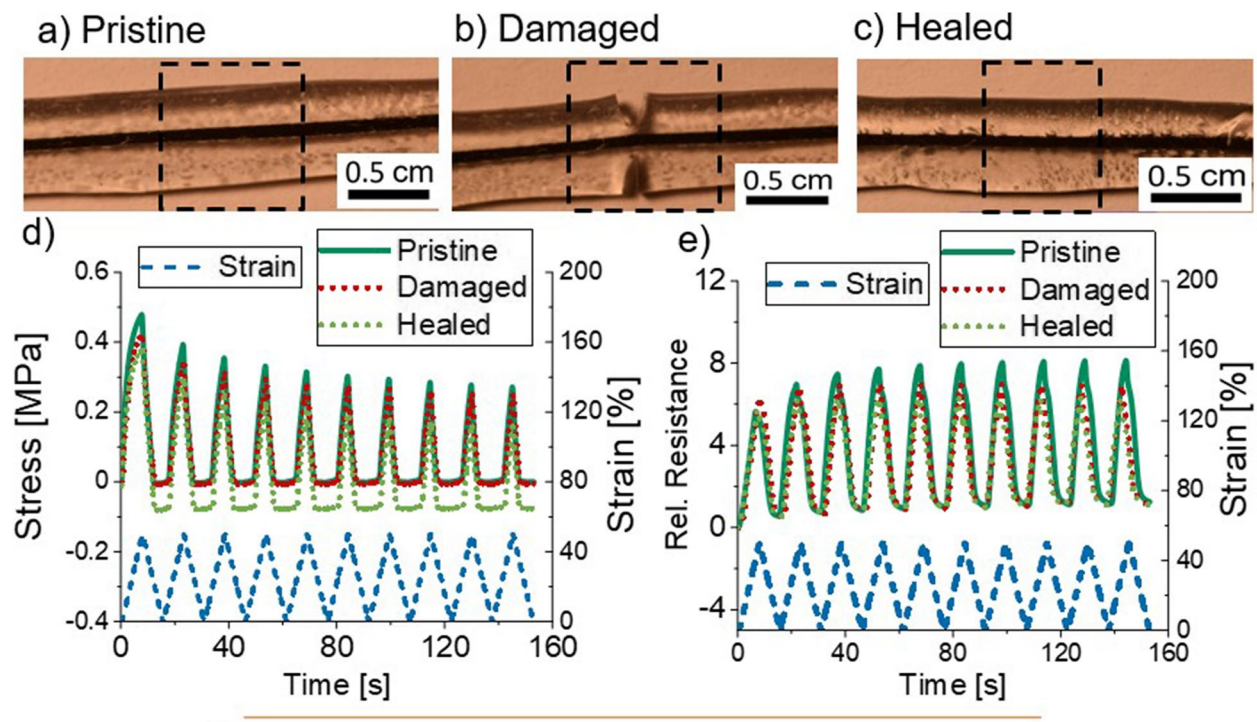

f)

	Pristine	Damaged	Healed
R_0 (kΩ)	1.4 ± 0.1	1.8 ± 0.2	1.4 ± 0.1
ΔR_{rel}	7.1 ± 0.4	6.4 ± 0.5	6.6 ± 0.3
Drift ΔR_{rel} 5-10 cycle (%)	1.1 ± 1	2.5 ± 1.5	2.2 ± 0

Fig. 10 Optical microscopy analysis of the SFC based on the supramolecular matrix UPy2 and the sensor fiber based on TPS 50A **a**) Pristine **b**) Damaged and **c**) Healed. Plots for the response of the **d**) Stress and **e**) Relative resistance **f**) Summary of the values for the R_0, ΔR_{rel} and the drift of the sensor signal between the 5th and 10th for the samples: pristine, damaged and healed

The drift remained low after the healing and the quality between the different samples is very consistent (low standard deviation).

Comparing the cycling experiments, for all SFCs, the R_0 can be used to monitor damage and healing steps directly. Using sensitivity (ΔR_{rel}) might be possible, but recalibration might be necessary, depending on the self-healing matrix. Overall, it is evident that the SH composites with the sensor fiber based on TPS 40A are not suitable, because after self-healing step they got too brittle to be further used in cycling tests. This fact was expected based on the brittleness of the elements based on TPS 40A, seen in Fig. 5 after heating at the 105 °C. Based on this observation, the sensor fibers and elements based on TPS 40A will not be used for further analysis.

Mechano-electrical behavior of the 3D printed sensing element composites (SECs)

In addition to the SFCs previously discussed, 3D printed sensor elements were integrated into the supramolecular matrix materials, namely UPy1 and UPy2. Even though the sensor elements based on TPS 40A resulted in higher sensitivity, sensor elements with TPS 50A were only integrated into the self-healing matrix materials, because of the brittle behavior after self-healing step. The results of the tensile testing tests are shown in Fig. 11.

From the response of the mechanical stress (Fig. 11a), it was seen that the slope of the stress–strain curve became negative for strains higher than 50% strain for the SEC UPy1 50A. The SEC UPy2 50A showed a strain hardening behavior that was also seen in the case of the sensor element based on TPS 50A. The same trend was seen in the case of the SFCs (Fig. 6). The elongation at the point of fracture at 370% strain was higher than the sensor element based on TPS 50A (240%), showing that the integration of the sensor element in the self-healing matrix has a positive effect on this property. The value is in the same range as the SFCs, showing for one more time that the self-healing matrix is the dominant influence in the mechanical behavior of the composite strip.

As for the electrical behavior (Fig. 11b), the SECs showed a positive piezoresistive response for the entire range of the sensor. The UPy2 50A strip showed better sensitivity at low strains (below 20%). The values of the GF are slightly lower than the value reported for the sensor element (14), but this behavior was also seen in the case of the SFCs. The values of the GF are in the same range, as the SFCs with the same self-healing elastomer matrix. Overall, despite the differences seen between sensor fibers and elements, the composite strips have similar mechanical and electrical behavior. The SFCs showed a slightly increased sensitivity

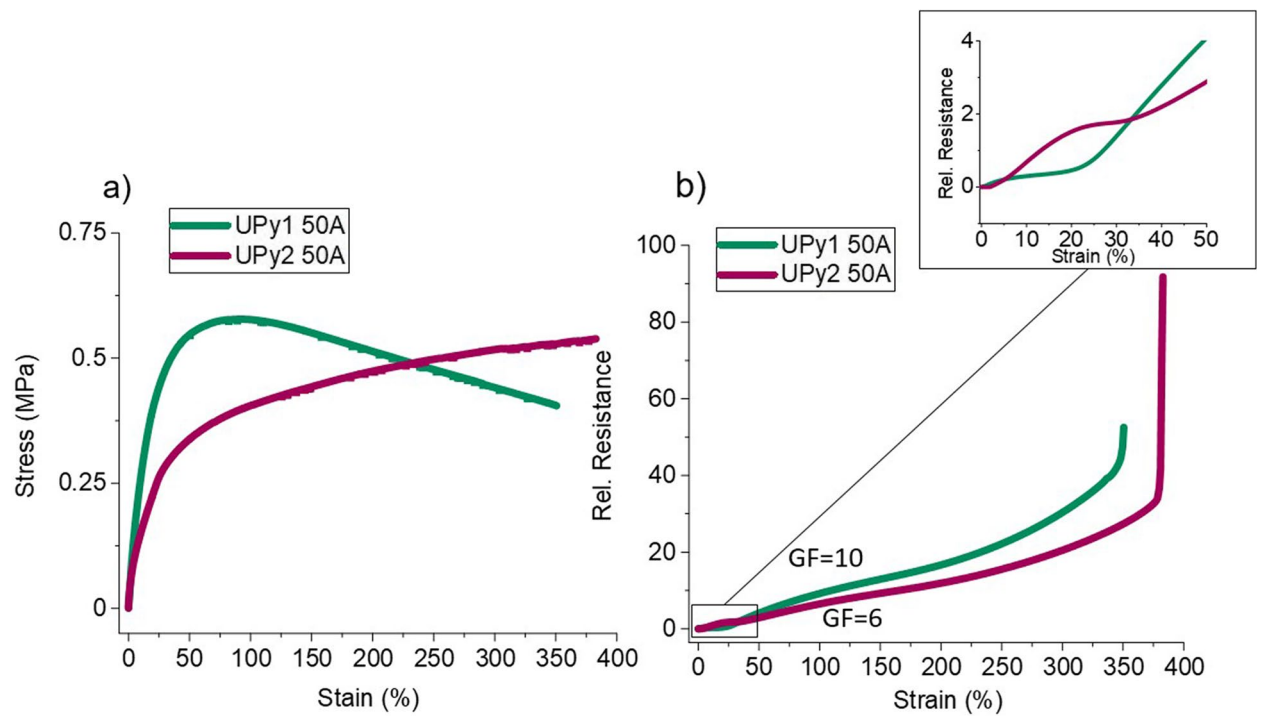

Fig. 11 **a** Stress–strain curve and **b** relative resistance curve for the self-healing sensor fiber composites (SFCs) with the supramolecular elastomers UPy1 and UPy2 for the TPS sensor elements with Shore hardness 50A during the tensile test up to the point fracture

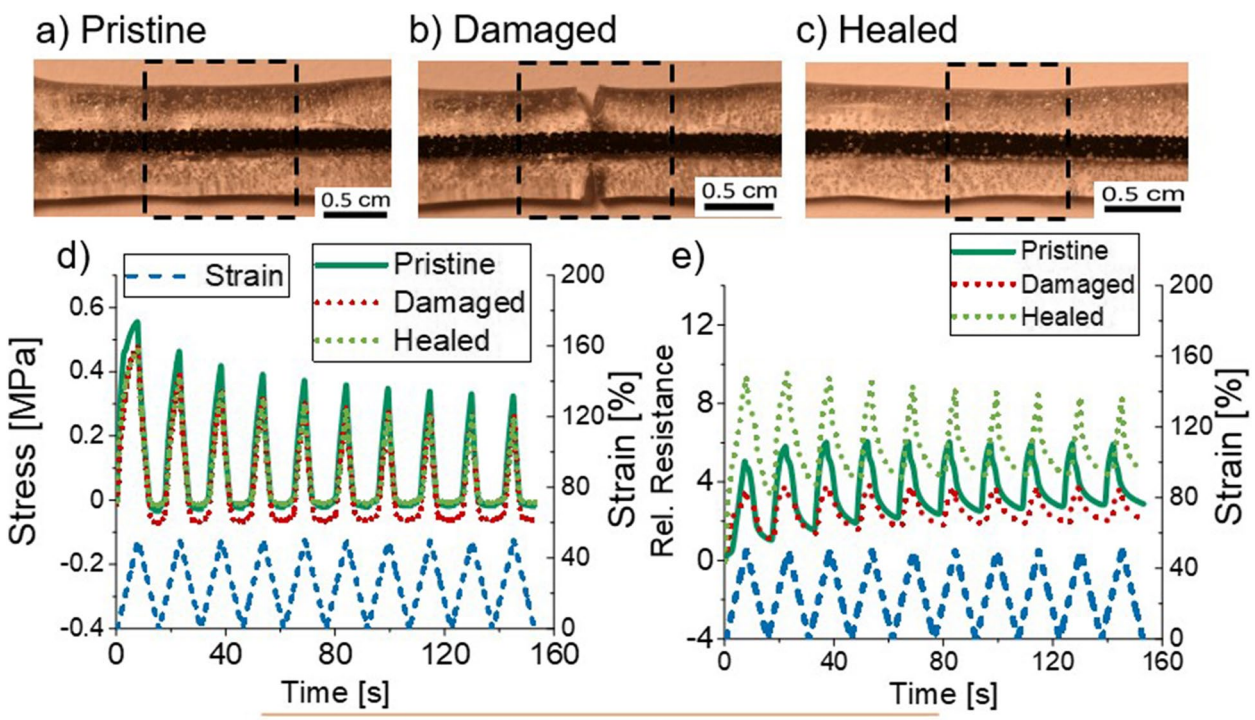

f)

	Pristine	Damaged	Healed
Ro (kΩ)	4.19 ± 0.1	7.2 ± 1	4.8 ± 0.4
ΔR_{rel}	3.5 ± 0.2	2.3 ± 0.3	4.1 ± 0.3
Drift R_{rel} 5-10 cycle (%)	18.5 ± 0.8	16.7 ± 0.4	16.9 ± 6

Fig. 12 Optical microscopy analysis of the SEC based on the supramolecular matrix UPy1 and the sensor element based on TPS 50A **a**) Pristine **b**) Damaged and **c**) Healed. Plots for the response of the **d**) Stress and **e**) Relative resistance **f**) Summary of the values for the R_0, ΔR_{rel} and the drift of the sensor signal between the 5th and 10th for the samples: pristine, damaged and healed

and the SECs a higher elongation at break, but in both cases, the differences are small.

Dynamic tensile testing results of the SECs are summarized in (Figs. 12a-f and 13a-f). The results are similar to those presented for the SFCs (Figs. 8 and 10). A calibration after the healing is needed for both the UPy1 50A and UPy2 50A SECs, since the value of the ΔR_{rel} does not recover after the healing. The UPy1 50A SEC showed a significant increase in the drift after the healing, a behavior also seen in the UPy1 50A SFC. The sensitivity (ΔR_{rel}) is higher for UPy2 50A SEC, but this behavior matches with the results seen in Fig. 11b for low strains. The values are in a similar range as the two SFCs.

It can be concluded that composite piezoresistive sensors by extrusion (fibers) or 3D printing (elements) can be used for monitoring self-healing materials. Since the value of the ΔR_{rel} does not recover after the healing (in all strips, but the UPy1 50A SFC), it is evident that recalibration after the healing step has to be performed for real applications, like closed-loop control systems for soft robots [41, 42].

SECs as composite strips for monitoring a soft robotic actuator module

In soft robotics, tendon or pneumatic bending actuators are often used [11, 28, 43, 44]. Due to the limited amount of self-healing material, the performance of the

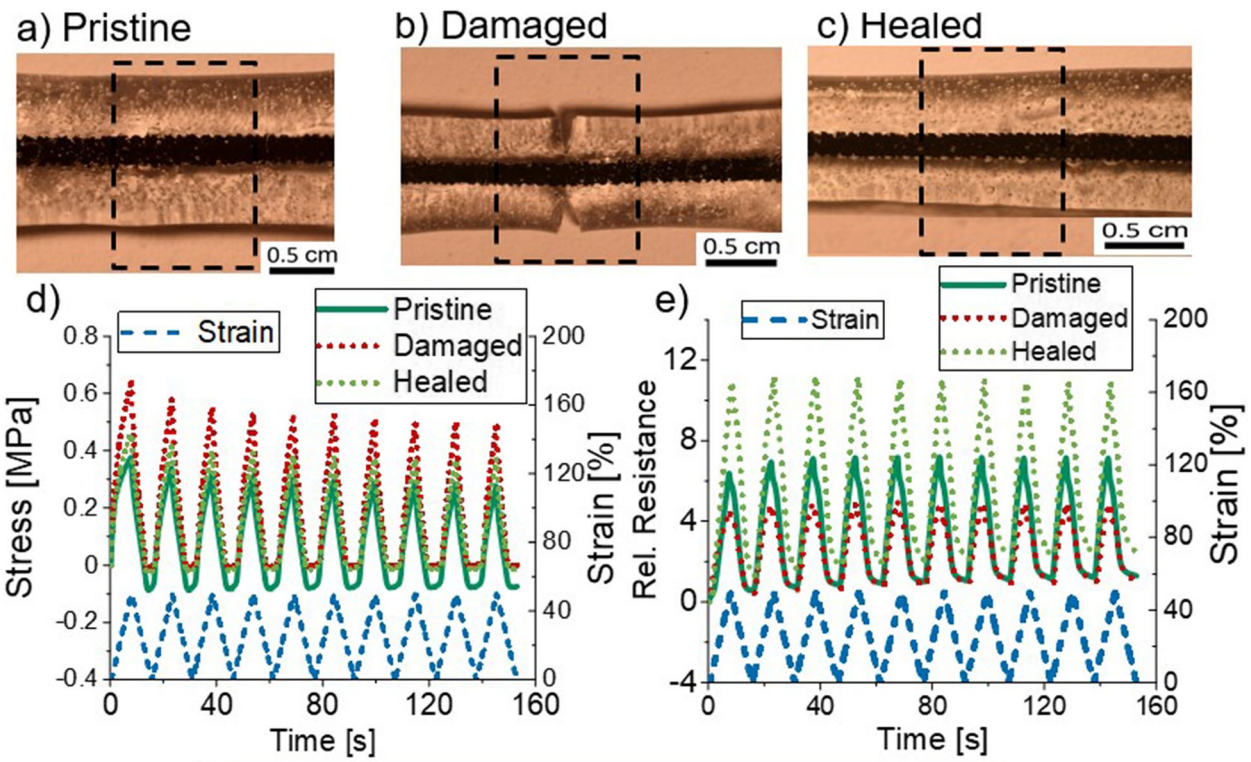

f)

	Pristine	Damaged	Healed
R_0 (kΩ)	2.7 ± 0.5	3.93 ± 0.6	3.1 ± 0.1
ΔR_{rel}	5.8 ± 0.4	4.1 ± 0.1	8.7 ± 0.4
Drift R_{rel} 5-10 cycle (%)	3.4 ± 1.3	3.8 ± 0.1	14.7 ± 11

Fig. 13 Optical microscopy analysis of the SEC based on the supramolecular matrix UPy2 and the sensor element based on TPS 50A **a** Pristine **b** Damaged and **c** Healed. Plots for the response of the **d** Stress and **e** Relative resistance **f** Summary of the values for the R_0, ΔR_{rel} and the drift of the sensor signal between the 5th and 10th for the samples: pristine, damaged and healed

SECs was investigated under bending conditions on a 3D printed TPU hinge (Fig. 14a-b). An internal setup was developed for the dynamic testing on tendon-driven hinges. The SECs were glued on the top of the hinge to investigate sensor signals in pristine, damaged and healed states (Fig. 14 c-d).

As expected from the cycling tensile experiments, the initial resistance R_0 can be used to monitor the different states (e.g. damage and healing) for the self-healing composite with both matrix materials. Even though the values were different for the two composites, the trend in the values was the same. For both the composites, the value of the R_0 increased when the damage occurred and returned to the initial values of the pristine after the healing (Fig. 14e and f). Remarkably for bending experiments, the drift of the electrical signal for both self-healing composites was significantly below 1% (e.g. 0.1%), including the first cycle. This is an improvement from the tensile experiments, where the values of the drift were, as high as 18%.

Conclusion

In this study, composite strips were developed by the integration of sensors in a self-healing matrix. Sensor fibers and 3D printed strips were compared for their piezoresistive response and damage detection in the self-healing matrix. It was seen that after the integration, the behavior of the composite strips was similar for both

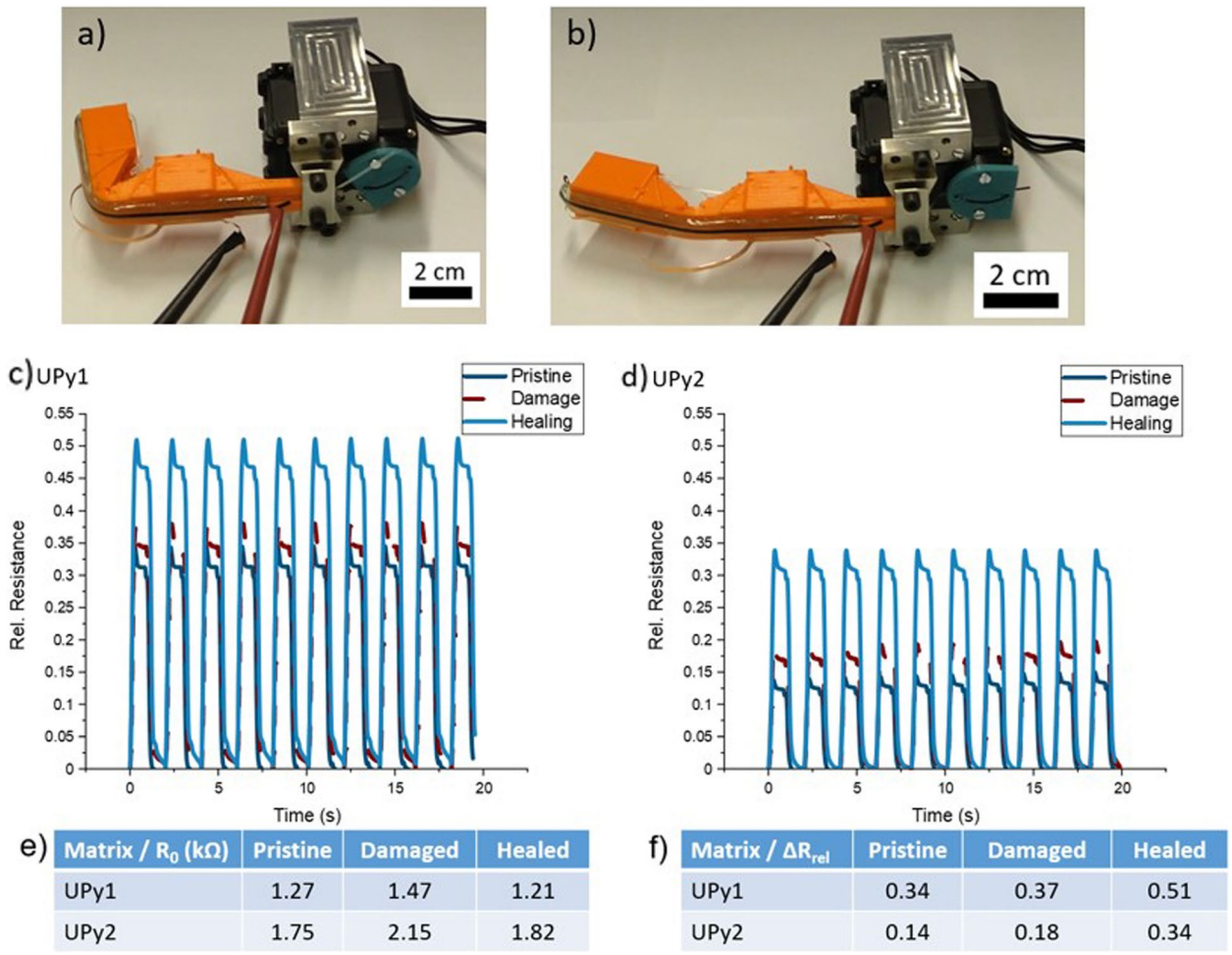

e)

Matrix / R_0 (kΩ)	Pristine	Damaged	Healed
UPy1	1.27	1.47	1.21
UPy2	1.75	2.15	1.82

f)

Matrix / ΔR_{rel}	Pristine	Damaged	Healed
UPy1	0.34	0.37	0.51
UPy2	0.14	0.18	0.34

Fig. 14 **a** The soft robotic actuator in position closed and **b**) position opened. The relative resistance response of the sensor element composites (SEC) based on TPS 50A in matrix **c**) UPy 1 and **d**) UPy 2. Summary of the values for the e) R_0 f) ΔR_{rel} for monitoring the position of a tendon-based soft robotic actuator module pristine, after damage and, after healing

sensor fibers and elements. The SFCs showed slightly better sensitivity and the SECs a higher elongation at break, but the values were very close for the two. Piezoresistive composites with TPS of two different Shore hardness values (40A and 50A) were investigated. The SFCs with the fiber of Shore hardness 40A could not be used after the healing, because the fiber became brittle after thermal treatment required healing. Therefore, only the 50A composition was suitable for the sensing element fabrication.

Both sensing element composites and fiber composites showed nociceptive properties for monitoring the damage and healing process by taking into account the value of the initial resistance (R_0). The initial resistance increased after the damage and recovered after the healing. However, a recalibration is necessary, as the relative resistance did not recover after the healing. The same observation was made with the experiments with the tendon-based soft robotic actuators, where the SECs were used. The sensors could monitor the position of the robots with a monotonic response and good reproducibility (drift smaller than 0.1%). Machine learning algorithms and AI developments can help cope with the re-calibration limitation, in the future.

Authors' contributions

A.G. and F.C. conceived and planned the experiments. A.G., H.K. and A.B. carried out the experiments. A.G., A.B. and F.C. contributed to the interpretation of the results. F.C. Supervised the project. A.G. and F.C. wrote the original draft of the manuscript. All authors provided critical feedback and helped shape the research, analysis and manuscript. The author(s) read and approved the final manuscript.

Funding
This project has received funding from the European Union's Horizon 2020 research and innovation programme under grant agreement No 828818 (SHERO Project).

Availability of data and materials
The data are available upon reasonable request from the authors.

Declarations

Competing interests
The authors have no interests to declare financial or otherwise.

Author details
[1]Department of Functional Materials, Empa – Swiss Federal Laboratories for Materials Science and Technology, Überlandstrasse 129, 8600 Dübendorf, Switzerland. [2]Brubotics, Vrije Universiteit Brussel (VUB), Pleinlaan 2, B-1050 Brussels, Belgium. [3]SupraPolix BV, Horsten 1, 5612AX Eindhoven, the Netherlands.

Received: 30 August 2022 Accepted: 19 December 2022
Published online: 26 December 2022

References

1. Y.J. Tan, J. Wu, H. Li, B.C.K. Tee, Self-Healing Electronic Materials for a Smart and Sustainable Future. ACS Appl. Mater. Interfaces **10**, 15331–15345 (2018)
2. A. Khan, N. Ahmed, M. Rabnawaz, Covalent Adaptable Network and Self-Healing Materials: Current Trends and Future Prospects in Sustainability. Polymers **12**, 2027 (2020)
3. R.J. Schwartzman, Pain and the Brain from Nociception to Cognition. Neurosurgery **38**, 1260–1260 (1996)
4. Elliott, P. The senses and survival: using a sensory homunculus to stimulate an exploration of adaptation. (1996) https://doi.org/10.1080/00219266.1996.9655476.
5. Macpherson, F. The Senses: Classic and Contemporary Philosophical Perspectives. (Oxford University Press, Oxford, 2011)
6. S. Dekoninck, C. Blanpain, Stem cell dynamics, migration and plasticity during wound healing. Nat Cell Biol **21**, 18–24 (2019)
7. C.J. Woolf, What is this thing called pain? J Clin Invest **120**, 3742–3744 (2010)
8. P.T. Coverley, W.J. Staszewski, Impact damage location in composite structures using optimized sensor triangulation procedure. Smart Mater. Struct. **12**, 795–803 (2003)
9. M. Khatib, O. Zohar, W. Saliba, H. Haick, A Multifunctional Electronic Skin Empowered with Damage Mapping and Autonomic Acceleration of Self-Healing in Designated Locations. Adv. Mater. **32**, 2000246 (2020)
10. A. Georgopoulou, A.W. Bosman, J. Brancart, B. Vanderborght, F. Clemens, Supramolecular Self-Healing Sensor Fiber Composites for Damage Detection in Piezoresistive Electronic Skin for Soft Robots. Polymers **13**, 2983 (2021)
11. A. Georgopoulou, B. Vanderborght, F. Clemens, Fabrication of a soft robotic gripper with integrated strain sensing elements using multi-material additive manufacturing. Frontiers in Robotics and AI **8**, 326 (2021)
12. A. Georgopoulou, S. Michel, F. Clemens, Sensorized Robotic Skin Based on Piezoresistive Sensor Fiber Composites Produced with Injection Molding of Liquid Silicone. Polymers **13**, 1226 (2021)
13. B.C.-K. Tee, C. Wang, R. Allen, Z. Bao, An electrically and mechanically self-healing composite with pressure- and flexion-sensitive properties for electronic skin applications. Nature Nanotech **7**, 825–832 (2012)
14. X. Zhang, Y. Song, F. Meng, G. Sun, L. Zhu, Optical fiber based soft curvature sensor with polyvinyl chloride reinforced silicone rubber substrate. Optik **178**, 567–574 (2019)
15. H.-R. Lim et al., Advanced Soft Materials, Sensor Integrations, and Applications of Wearable Flexible Hybrid Electronics in Healthcare, Energy, and Environment. Adv. Mater. **32**, 1901924 (2020)
16. S. Chun, Y. Choi, W. Park, All-graphene strain sensor on soft substrate. Carbon **116**, 753–759 (2017)
17. A. Georgopoulou, S. Michel, B. Vanderborght, F. Clemens, Piezoresistive sensor fiber composites based on silicone elastomers for the monitoring of the position of a robot arm. Sens. Actuators, A **318**, 112433 (2021)
18. T. Dong, Y. Gu, T. Liu, M. Pecht, Resistive and capacitive strain sensors based on customized compliant electrode: Comparison and their wearable applications. Sens. Actuators, A **326**, 112720 (2021)
19. D. Jiang et al., Flexible Sandwich Structural Strain Sensor Based on Silver Nanowires Decorated with Self-Healing Substrate. Macromol. Mater. Eng. **304**, 1900074 (2019)
20. J. Chen, J. Liu, T. Thundat, H. Zeng, Polypyrrole-Doped Conductive Supramolecular Elastomer with Stretchability, Rapid Self-Healing, and Adhesive Property for Flexible Electronic Sensors. ACS Appl. Mater. Interfaces **11**, 18720–18729 (2019)
21. J. Hua Xu, S. Ye, C. Di Ding, L. Hua Tan, J. Jun Fu, Autonomous self-healing supramolecular elastomer reinforced and toughened by graphitic carbon nitride nanosheets tailored for smart anticorrosion coating applications. J. Mater. Chem. A **6**, 5887–5898 (2018)
22. K. Zhang et al., A NIR laser induced self-healing PDMS/Gold nanoparticles conductive elastomer for wearable sensor. J. Colloid Interface Sci. **599**, 360–369 (2021)
23. K. Zhang et al., A stretchable and self-healable organosilicon conductive nanocomposite for a reliable and sensitive strain sensor. J. Mater. Chem. C **8**, 17277–17288 (2020)
24. S.R. Khimi, S.N. Syamsinar, T.N.L. Najwa, Effect of Carbon Black on Self-healing Efficiency of Natural Rubber. Materials Today: Proceedings **17**, 1064–1071 (2019)
25. Y. Han, X. Wu, X. Zhang, C. Lu, Self-Healing, Highly Sensitive Electronic Sensors Enabled by Metal-Ligand Coordination and Hierarchical Structure Design. ACS Appl. Mater. Interfaces **9**, 20106–20114 (2017)
26. X. Liu, C. Lu, X. Wu, X. Zhang, Self-healing strain sensors based on nanostructured supramolecular conductive elastomers. J. Mater. Chem. A **5**, 9824–9832 (2017)
27. X. Dai, L.-B. Huang, Y. Du, J. Han, J. Kong, Self-healing flexible strain sensors based on dynamically cross-linked conductive nanocomposites. Composites Communications **24**, 100654 (2021)
28. A. Georgopoulou, L. Egloff, B. Vanderborght, F. Clemens, A Sensorized Soft Pneumatic Actuator Fabricated with Extrusion-Based Additive Manufacturing. Actuators **10**, 102 (2021)
29. A. Georgopoulou, F. Clemens, Pellet-based fused deposition modeling for the development of soft compliant robotic grippers with integrated sensing elements. Flex. Print. Electron. **7**, 025010 (2022)
30. Z. Zou et al., Rehealable, fully recyclable, and malleable electronic skin enabled by dynamic covalent thermoset nanocomposite. Sci. Adv. **4**, eaaq0508 (2018)
31. J. Byun et al., Electronic skins for soft, compact, reversible assembly of wirelessly activated fully soft robots. Sci. Robotics **3**, eaas9020 (2018)
32. B. Ying, X. Liu, Skin-like hydrogel devices for wearable sensing, soft robotics and beyond. iScience **24**, 103174 (2021)
33. J. Langenbach et al., Adhesion and Stiffness Matching in Epoxy-Vitrimers/Strain Sensor Fiber Laminates. ACS Appl. Polym. Mater. **4**, 1264–1275 (2022)
34. C. Mattmann, F. Clemens, G. Troester, Sensor for measuring strain in textile. Sensors **8**, 3719–3732 (2008)
35. M. Melnykowycz, B. Koll, D. Scharf, F. Clemens, Comparison of Piezoresistive Monofilament Polymer Sensors. Sensors **14**, 1278–1294 (2014)
36. Georgopoulou, A., Sebastian, T. & Clemens, F. J. Thermoplastic elastomer composite filaments for strain sensing applications extruded with an FDM 3D printer. Flex. Print. Electron. (2020) https://doi.org/10.1088/2058-8585/ab9a22.
37. G.M.L. van Gemert, J.W. Peeters, S.H.M. Söntjens, H.M. Janssen, A.W. Bosman, Self-Healing Supramolecular Polymers In Action. Macromol. Chem. Phys. **213**, 234–242 (2012)
38. Terryn, S., Brancart, J., Lefeber, D., Assche, G. V. & Vanderborght, B. Self-healing soft pneumatic robots. Science Robotics 2, (2017).
39. S. Terryn et al., A review on self-healing polymers for soft robotics. Mater. Today **47**, 187–205 (2021)
40. Clemens, F. J. et al. Development of Piezoresistive Fiber Sensors, Based on Carbon Black Filled Thermoplastic Elastomer Compounds, for Textile Application. 80, 7. (2012)

41. T.G. Thuruthel, E. Falotico, F. Renda, C. Laschi, Model-Based Reinforcement Learning for Closed-Loop Dynamic Control of Soft Robotic Manipulators. IEEE Trans. Rob. **35**, 124–134 (2019)
42. A. Zolfagharian, A. Kaynak, A. Kouzani, Closed-loop 4D-printed soft robots. Mater. Des. **188**, 108411 (2020)
43. T. Giffney et al., Soft Pneumatic Bending Actuator with Integrated Carbon Nanotube Displacement Sensor. Robotics **5**, 7 (2016)
44. Giffney, T. et al. Soft pneumatic bending actuator with integrated carbon nanotube displacement sensor. (2016) https://doi.org/10.3390/robotics5010007.

Publisher's Note